Analytical Biochemistry **2008,** *374,* 143–153

doi: 10.1016/j.ab.2007.10.035

Label-free electrical detection of DNA hybridization for the example of influenza virus gene sequences

Andreas Kukol [a,*], *Peng Li* [b], *Pedro Estrela* [b], *Paul Ko-Ferrigno* [c,1], *Piero Migliorato* [b]

[a] School of Life Sciences, University of Hertfordshire, Hatfield AL10 9AB, UK

[b] Centre for Advanced Photonics and Electronics, Electrical Engineering Division, Department of Engineering, University of Cambridge, Cambridge CB3 0FA, UK

[c] Hutchison/MRC Research Centre and Cancer Cell Unit, Cambridge CB2 0XZ, UK

[*] Corresponding author. a.kukol@herts.ac.uk

[1] Current address: Leeds Institute of Molecular Medicine, St. James University Hospital, Leeds LS9 7TF, UK

ABSTRACT

Microarrays based on DNA–DNA hybridization are potentially useful for detecting and subtyping viruses but require fluorescence labeling and imaging equipment. We investigated a label-free electrical detection system using electrochemical impedance spectroscopy that is able to detect hybridization of DNA target sequences derived from avian H5N1 influenza virus to gold surface-attached single-stranded DNA oligonucleotide probes. A 23-nt probe is able to detect a 120-nt base fragment of the influenza A hemagglutinin gene sequence. We describe a novel method of data analysis that is compatible with automatic measurement without operator input, contrary to curve fitting used in conventional electrochemical impedance spectroscopy (EIS) data analysis. A systematic investigation of the detection signal for various spacer molecules between the oligonucleotide probe and the gold surface revealed that the signal/background ratio improves as the length of the spacer increases, with a 12- to 18-atom spacer element being optimal. The optimal spacer molecule allows a detection limit between 30 and 100 fmol DNA with a macroscopic gold disc electrode of 1 mm radius. The dependence of the detection signal on the concentration of a 23-nt target follows a binding curve with an approximate 1:1 stoichiometry and a dissociation constant of K_D = 13 ± 4 nM at 295 K.

KEYWORDS

DNA; Biosensor; Avian influenza; Label-free detection; Electrochemical impedance spectroscopy; Sulfhydryl chemistry; Spacer molecule; Oligonucleotide.

A possible application for a label-free electrical detection system is the avian influenza virus (AIV), which circulates in wild and domestic bird populations and currently is considered as a potential source for a new influenza pandemic. Influenza viruses belong to the family of Orthomyxoviridae and are classified into types A, B, and C based on the antigenic properties of their nucleoprotein and matrix protein. Further subtyping of influenza A viruses is based on the antigenic properties of the outer surface glycoproteins hemagglutinin (HA) and neuraminidase (NA) given as HxNy subtype. So far, 16 HA (H1–H16) and 9 NA (N1–N9) subtypes have been identified, although not all combinations of HxNy occur naturally. The influenza A virus is a lipid enveloped virus containing a negative sense RNA genome with a total length of approximately 13.6 kb organized into eight separate RNA molecules (segments) that code for 11 proteins [1,2].

Influenza viruses cause a respiratory disease in humans resulting in an average death toll of 36,000 people each year in the United States alone [3]. Apart from annually recurring epidemics, influenza A viruses, which infect avian and mammalian species, have been responsible for devastating pandemics killing at least 40 million people in 1918–1919 (Spanish flu, H1N1) [4] and less serious pandemics in 1957 (Asian influenza, H2N2), 1968 (Hong Kong influenza, H3N2), and 1977 (Russian influenza, H1N1) [5]. Influenza pandemics seem to occur when a highly pathogenic avian type virus acquires the capability of efficient human-to-human transmission (reviewed in Ref. [6]). A current threat is an avian H5N1 virus that emerged in May 1997 [7,8] and has caused nearly 90 human deaths, with the most devastating outbreak occurring in Asia in 2003–2004 [9]. Horimoto and Kawaoka discussed the possibility that avian H5N1 could give rise to a new pandemic if it acquires the capacity of efficient human-to-human transmission [6]. This threat makes it necessary to detect highly pathogenic avian influenza viruses as early as possible, ideally in the field using portable detection devices.

Classical methods of influenza virus diagnostics are based on virus isolation, culture, and subtype identification by immunoassays, possibly followed by an in vivo experiment, to determine pathogenicity [10]. This process requires 3 to 7 days of virus culture in addition to transporting the sample to the laboratory. Faster molecular methods based on reverse transcription–polymerase chain reaction (RT–PCR) [11–14], which require the decision prior to testing for which subtype the test should be carried out, are available. Recently, Hoffmann and coworkers described a cascade of real-time RT–PCRs (rRT–PCRs) that determines in the first step the presence of influenza A sequences by rRT–PCR specific to the matrix gene and, if positive, is followed by rRT–PCRs targeted at H7- and H5-specific sequences [15]. Where the H5 sequence is found, an rRT–PCR assay specifically detects highly pathogenic H5N1 strains of the Quinghai lineage that are representative of strains currently occurring in Europe [15]. Portable RT–PCR systems have been described and applied, for example, to the swine fever virus [16]. As an alternative, DNA microarrays have been proposed for complete subtyping and additional virus information [17– 21]. Current microarray technology is based on amplification of virus RNA into complementary DNA (cDNA) by RT–PCR, with the incorporation of fluorescently labeled bases into the cDNA to allow subsequent optical detection of hybridization between labeled virus-derived target cDNA and on-chip immobilized probe oligonucleotides. Microarray technology is in principle more powerful than currently established techniques, allowing complete subtype identification and even short sequence information to be obtained from limited quantities of sample [20]. However, current microarray platforms require RT–PCR amplification and fluorescence imaging of the array, which is possible only with dedicated equipment available in a diagnostic lab, precluding field-testing of domestic bird populations on a global scale.

One solution to this problem would be the development of inexpensive portable devices

incorporating a disposable sensing element. In this study, we investigated the application of Faradaic electrochemical impedance spectroscopy (EIS) to detect avian influenza gene sequences without the need for target labeling or fluorescence imaging equipment. EIS (reviewed in Refs. [22,23]) provides detailed information about the electrical resistance and capacitance of conducting and nonconducting surfaces immersed in an electrolyte. Changes to the surface can be measured as changes in the electrical parameters of the system. The hybridization of target DNA to surfaceattached probe DNA leads to an increase in negative charge on the surface, which prevents the access of negatively charged probe molecules (e.g., the redox couple $[Fe(CN)_6]^{3-}/[Fe(CN)_6]^{4-}$) to the surface due to electrostatic repulsion [24,25]. Label-free impedance detection of oligonucleotide hybridization has been described, for example, for interdigitated ultramicroelectrodes [26] or for electrical microarrays using a coulostatic pulse technique [27].

The electrochemical impedance spectrum is obtained by measuring the electrical current response in dependence of the frequency of the applied voltage. In any electrical circuit composed of capacitive and resistive elements exposed to an alternating voltage, there will be a phase difference between the electrical current and the applied voltage in dependence of the frequency *f*. This is conveniently represented by the complex impedance *Z*:

$$Z(f) = Z' + jZ'' \qquad (1)$$

where *j* represents the imaginary unit $j = \sqrt{(-1)}$. The data typically are displayed in a plot of $-Z''$ against Z' called a Nyquist plot (Fig. 1A). Although this does not show the frequency dependence of the impedance directly, data points obtained at the highest frequencies are in the leftmost part of the plot and those obtained at the lowest frequencies are at the right-hand side of the plot. The curve can be fitted to a model of an electrical equivalent circuit (Fig. 1B), allowing interpretation of the surface properties of the device in terms of electrical circuit elements. One drawback of this approach is that interpretation of the data requires an iterative curve-fitting algorithm and user input that is not readily accommodated in a mobile device.

For oligonucleotide probes attached via –SH groups to the surface of gold electrodes, our results show significant changes in the EIS curves on hybridization with target sequences. The quality and magnitude of the detection signal depend on the

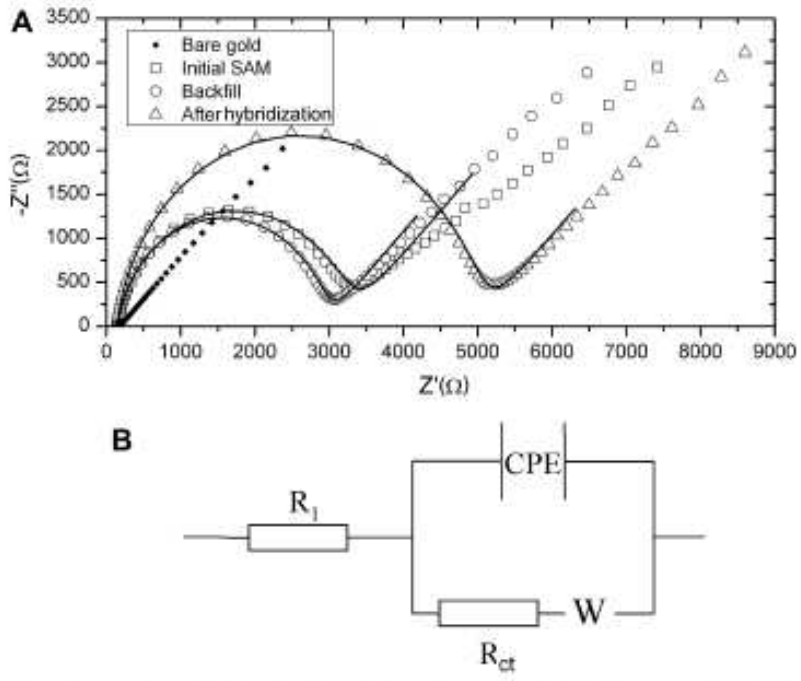

Fig. 1. Nyquist plot of typical impedance spectra. (A) Nyquist plots after various stages of electrode preparation, the bare gold surface (■), after the preparation of the SAM (□), after further treatment with mercaptohexanol (backfilling) (○), and after hybridization with cHA23 (Δ). The solid lines show the curve fit of the electrical equivalent circuit in panel B to the data. (B) Model electrical equivalent circuit to describe the data shown in panel A. R_1, electrolyte resistance; R_{ct}, charge transfer resistance; CPE, constant phase element; *W*, Warburg impedance.

nature and length of various spacers between the -SH group and the oligonucleotide. We have devised a novel procedure for data analysis that does not require curve fitting or human intervention and, therefore, is particularly suited for a portable field device. The detection limit for a 23-nt DNA sequence derived from a highly pathogenic H5N1 AIV strain is between 30 and 100 fmol.

Materials and methods

Selection of oligonucleotides

Virus gene sequences were obtained from the National Center for Biotechnology Information's (NCBI) Influenza Virus Resource [28] and further processed with BioEdit software (version 7.0.5.3) [29,30]. Multiple sequence alignment was performed with MUSCLE (version 3.6) [31,32].

The majority of sulfhydryl-modified oligonucleotide probes were obtained from Eurogentec (Seraing, Belgium), and unmodified target oligonucleotides were obtained from MWG Biotech (London, UK). The probes MA20/S18/C6 and HA23/S18/C6 were obtained from the Protein and Nucleic Acid Chemistry Facility at the University of Cambridge.

Preparation of electrodes

Gold disk working electrodes with a radius of 1 mm were obtained from CH Instruments (Austin, TX, USA) and polished with aluminum oxide particles of 5 μm diameter (Buehler, Lake Bluff, IL, USA) followed by sonication in water using a conventional sonicator (150 W power output), then polished with 1-μm particles followed by sonication in water/detergent, then polished with 0.3-μm particles followed by sonication in water, and finally polished with a soft pad (Buehler) followed by sonication in water. They were further cleaned electrochemically in 0.5 M H_2SO_4 by cyclic voltammetry, varying the potential between -0.05 and +1.1 V against an Hg/Hg_2SO_4 reference electrode for 60 cycles using a three-electrode cell with the gold electrode as the working electrode and a platinum wire as the counter electrode. The electrodes were connected to an Autolab PGSTAT302 potentiostat (Eco Chemie, Utrecht, Netherlands). For self-assembled monolayer (SAM) formation and oligonucleotide immobilization, the electrode was dried briefly in a stream of nitrogen and then incubated for 20 h in a hydration chamber at 22°C with 20 μl of a buffer solution of 100 mM Tris–hydroxymethyl- aminoethane (pH 8.5), 100

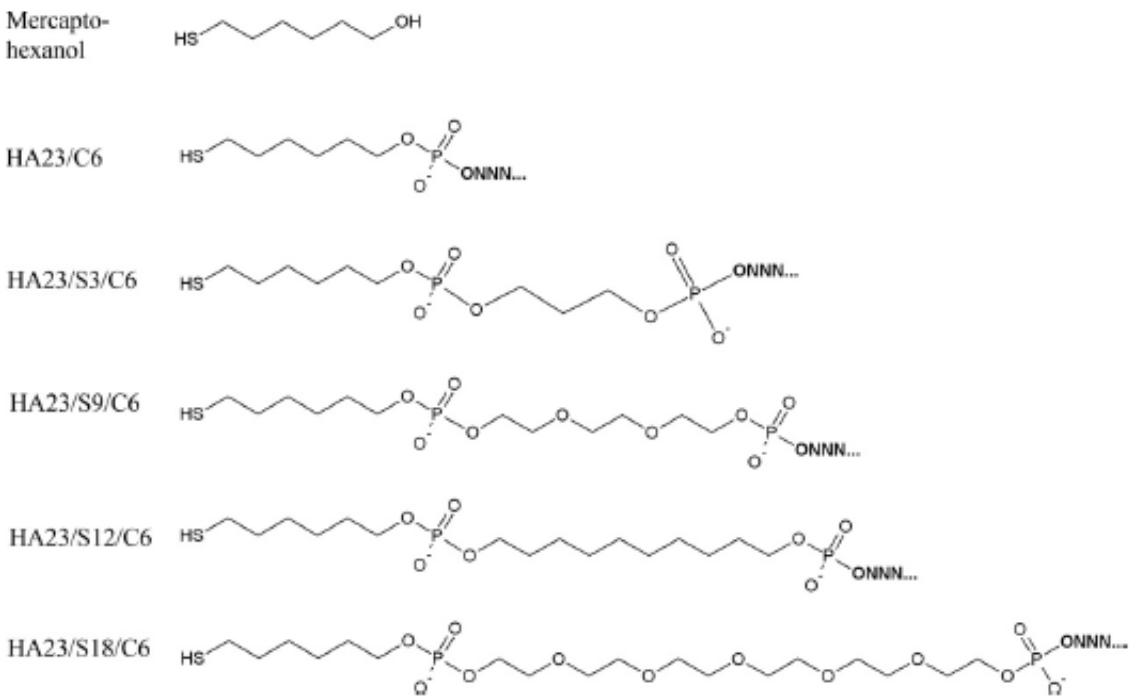

Fig. 2. Probe molecules. Chemical structure of the probe molecules and the backfilling agent mercaptohexanol used in this study with the abbreviations (left-hand side) used in the text. NNN... denotes the single-stranded oligonucleotide sequence. The sulfhydryl group is always at the end of a 6-carbon chain, at the end of which is attached the variable spacer. The spacer is formed either by pure carbon chains (C_3 or C_{12}) or mixed carbon/oxygen chains of 9 or 18 atoms in total.

mM NaCl, and 5 mM $MgCl_2$ containing 10 µM mercaptohexanol and 1 µM sulfhydryl-modified DNA oligonucleotide (Fig. 2). The electrode was then rinsed for 2 min in rinse buffer (100 mM phosphate buffer [pH 7.2], 100 mM NaCl, and 5 mM MgCl2) before measurement of the impedance spectrum. The impedance spectrum was measured with the Autolab PGSTAT302 in a solution of 5 mM $K_4[Fe(CN)_6]$, 5 mM $K_3[Fe(CN)_6]$, and 100 mM phosphate buffer at pH 7.2 using the three-electrode cell described above, and the reference electrode was connected via a salt bridge filled with 100 mM phosphate buffer. The impedance spectrum was measured in the frequency range from 100 kHz to 100 mHz, and a potential of -0.195 V versus the reference electrode was applied, corresponding to the formal potential of the redox couple.

For backfilling, the electrode was treated for 2 h in 20 µl of a solution of 1 mM mercaptohexanol, 100 mM phosphate buffer (pH 7.2), 100 mM NaCl, and 5 mM $MgCl_2$ in a hydration chamber at 22°C, followed by measurement of the impedance spectrum as described above.

Sensing of target oligonucleotides

The prepared gold electrode surface was covered with 20 µl of a solution of target oligonucleotides of variable concentrations (see Results) in 100 mM phosphate buffer (pH 7.2), 100 mM NaCl, and 5 mM $MgCl_2$ for 2 h at 22°C in a hydration chamber. The minimum amount of solution necessary to cover the surface was estimated to be 10 µl, although 20 µl has always been used. Then the electrode was rinsed for 2 min in the same buffer without oligonucleotide and the impedance spectrum was measured as described above.

Data analysis

Curve fitting of the impedance spectra to an electrical equivalent circuit was performed with the Frequency Response Analyzer software supplied with the Autolab potentiostat (Eco Chemie). Only impedances obtained at frequencies between 0.1 Hz and 10 kHz were used for curve fitting so as to avoid contributions from the electrochemical cell and connecting wires at high frequencies and the influence of DC conductivity of the electrolyte solution at low frequencies. The normalized hybridization signal was obtained by converting the Autolab data files into space delimited ASCII files and subsequent calculation of the signal using a computer program developed in our lab.

The concentration dependence of signal S was fitted with a binding curve for the reaction between probe P and target R, that is, $P + rT \rightarrow PT_r$:

$$S = S_{max}[\text{cHA23}]^r / (K_D{}^r + [\text{cHA23}]^r); \qquad (2)$$

where S_{max} is the maximum signal for [cHA23]→∞, r is the stoichiometric factor, and K_D is the dissociation constant of PT_r.

Results

Selection of probe and target oligonucleotide sequences

Highly pathogenic avian influenza viruses have been found to possess several basic amino acids inserted into the posttranslational cleavage site of the HA precursor protein [33]. Therefore, we selected an amino acid sequence typical of highly pathogenic viruses, PQRERRRKKR, which occurs in 498 of 8051 available HA sequences from the NCBI's Influenza Virus Resource [28]. In particular, this sequence occurs in an avian H5N1 virus isolated from a human in 1997, A/Hong Kong/503/97 (GenBank accession no. AF102679). The reverse translation of this sequence into DNA yields the 30-nt sequence 50-cctcaaaga gagagaagaagaaaaaagagagga-30, which is found in 438 H5N1 sequences from virus isolates between 1997 and 2006. To detect a larger number of virus isolates, we truncated the sequence to the 23-nt fragment 50-cctcaaagagaga gaagaagaaa-30 (designated here HA23), which occurs in 586 virus isolates [28], potentially enabling a future biosensor to detect a larger number of highly pathogenic

Table 1
DNA oligonucleotide probes and targets

Name	Function	Sequence (5′ → 3′)
HA23	Probe for pathogenic avian H5N1 hemagglutinin gene sequence	5′-cctcaaagagagagaagaagaaa-3′
MA20	Probe for influenza A matrix protein gene sequence	5′-gtgagcgaggactgcagcgt-3′
cHA23	Target, reverse complement to HA23	5′-tttcttcttctctctctttgagg-3′
cHA120	Long target sequence with 23-nt reverse complementary to HA23	5′-ccatcctcccctctataaaacctgc tatagctccaaataatcctctct ttttttcttctctctctttga ggctatttctgagcccagtcgcaa ggactaatctgtttgatttcacata-3′
cMA20	Target, reverse complement to MA20	5′-acgctgcagtcctcgctcac-3′

viruses. This sequence, however, has 101 significant matches in the ‘‘whole genome shotgun sequence’’ database of the NCBI; thus, positive detection events due to other genes in the environment cannot be excluded with a single probe. To detect influenza A viruses specifically, we selected a 20-nt sequence from an invariant portion of the matrix gene (MA), gtgagcgaggactgcagcgt (MA20), which also has a number of matches with noninfluenza genes but, most important, no double matches with the HA23 sequence.

To model negative strand influenza virus RNA, we designed two short target oligonucleotides, cHA23 and cMA20, which are the reverse complement to the probe sequences HA23 and MA20 (Table 1). A more realistic scenario encountered in environmental samples is longer target RNA fragments likely to be generated by sample degradation. Thus, we designed a 120-nt oligonucleotide derived from the hemagglutinin gene that contains 23 nucleotides reverse complementary to HA23 (cHA120) (Table 1).

Electrochemical characterization of the biosensing event

The Faradaic impedance spectra of gold disc electrodes with a radius of 1 mm were obtained in the presence of the negatively charged redox couple $[Fe(CN)_6]^{3-}/[Fe(CN)_6]^{4-}$ at various stages of the electrode preparation process (Fig. 1A). The spectra of modified electrodes show two components: a semicircle followed by a linear increasing portion. The unmodified gold electrode showed a barely visible semicircle at higher frequencies, followed by a linear part that covers most of the spectrum. Overnight treatment of the gold electrode with an aqueous buffer containing a mixture of 10 μM mercaptohexanol and 1 μM of an –SH-labeled oligonucleotide (HA23/S12/C6 [see Fig. 2]) at pH 8.5 resulted in a clear change of the curve, with a significant semicircle portion followed by a linear increasing portion. The curve did not change on rinsing with buffer, indicating the formation of a mixed oligonucleotide/mercaptohexanol SAM on the gold surface. Subsequent treatment of the gold surface with 1 mM mercaptohexanol for 2 h (backfilling) resulted in a reduction of the semicircle diameter, but overall only a relatively small change was observed.

For the biosensing event, the electrode was incubated for 2 h with a reverse complementary target cHA23 (Table 1). The Nyquist plot (Fig. 1A) showed a significant change of the curve caused by an increased diameter of the semicircle compared with the plot obtained before treatment with the target oligonucleotide.

The data were modeled with a Randles and Ershler electronic equivalent circuit [34,35] shown in Fig. 1B. R_1 represents the ohmic resistance of the electrolyte solution, and the Warburg impedance W results from the diffusion of ions from the bulk electrolyte to the gold surface. The constant phase element (CPE) represents the combined capacitance of the SAM and the electrochemical cell, and R_{ct} is the resistance for charge transfer from solution to the electrode caused by the electrochemical double layer and the negatively charged oligonucleotides repelling the negatively charged redox probe molecule. The use of a CPE instead of a capacitor resulted in better fits, likely because the CPE represents the nonhomogeneity of the electrode surface. The extent of deviation

Table 2
Fit parameters for curves in Fig. 1

Experiment	R_1 (Ω) (±2%)	CPE (μS s^n) (±5%)	n (±1%)	W (mS $s^{1/2}$) (±8%)	R_{ct} (kΩ) (±2%)	C_{calc} (μF)[a]
SAM preparation	150	0.8879	0.8892	0.5166	3.067	0.4254
Backfilling	156	0.5962	0.9176	0.7104	2.776	0.3355
Hybridization	143	0.5585	0.9235	0.6716	4.85	0.3423

Note. The meanings of the variables are explained in Fig. 1.
[a] The capacitance has been calculated according to the relationship $C_{calc} = (\text{CPE } R_{ct})^{1/n}/R_{ct}$ [41].

from an ideal capacitor can be modeled by a parameter n ($0 \le n \le 1$), where $n = 1$ for an ideal capacitor [36]. The parameters of the fit (Table 2) show that the biosensing of DNA hybridization was characterized by a marked increase in the electron transfer resistance from R_{ct} = 2.78 kΩ to R_{ct} = 4.85 kΩ (i.e., a 75% increase), whereas the parameters of the CPE changed slightly. The calculated capacitance decreased slightly. The pattern of relative change in the parameters for each electrode on hybridization with a complementary DNA oligonucleotide was similar for all experiments with the same spacer molecule, but the electrochemical characteristics of the SAM before hybridization show large variations in the electron transfer resistance from Rct = 1.0 kΩ to Rct = 7.0 kΩ.

Treatment of the SAM with a noncomplementary DNA sequence resulted in an insignificant shift of the curve in the Nyquist plot (see Fig. 4A later). However, the change in electrical signal in detail on hybridization or on treatment with a noncomplementary sequence depended on the nature and length of the spacer molecule (Fig. 2) between the oligonucleotide probe and the gold surface, which is described below.

In a similar experiment, we demonstrated the detection of a gene sequence from the influenza matrix protein cMA20 using the 20-mer oligonucleotide MA20/S18/C6 as a probe attached to the gold surface. The charge transfer resistance changed from R_{ct} = 6.59 kΩ to R_{ct} = 9.89 kΩ (i.e., by 50%) on treatment with cMA20 (Fig. 3A), whereas the charge transfer resistance increased only from R_{ct} = 5.38 kΩ to R_{ct} = 5.98 kΩ for a different electrode treated with cHA23 (Fig. 3B).

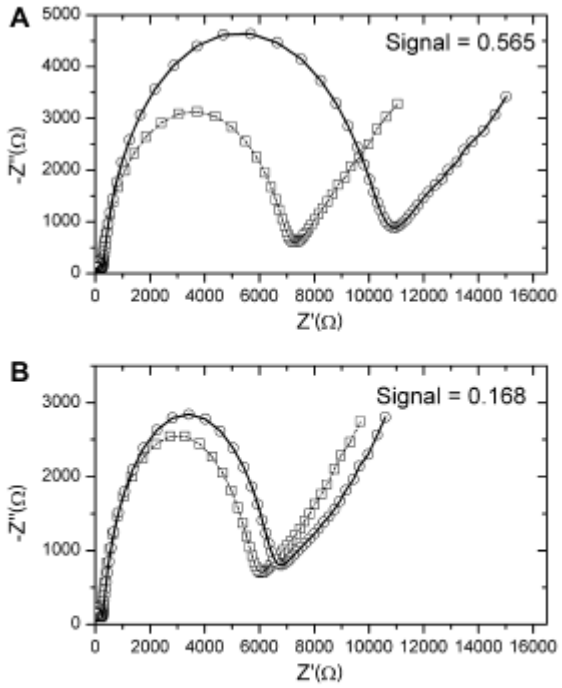

Fig. 3. Detection of cMA20. (A) EIS of a gold electrode with MA20/S18/C6 probes before (□) and after (○) treatment with reverse complementary target cMA20. The signal obtained from the model-free data analysis is given. (B) EIS of a gold electrode with MA20/S18/C6 probes before (□) and after (○) treatment with noncomplementary target cHA23.

Automated data analysis

The curve fitting of the impedance spectra illustrated above requires a complex fitting algorithm and human intervention for the setting of starting values. For a biosensor that can be used in the field, an automatic procedure for obtaining the signal using an algorithm with a minimal amount of calculations is desirable. We achieve this by using the modulus of the impedance $|Z|_f$ in dependence of frequency f of the alternating voltage. From the complex impedance defined in Eq. (1), the modulus is obtained as

$$|Z|_f = (Z'^2 + Z''^2)^{1/2} \quad (3)$$

The hybridization signal is calculated from the sum over N data points of the absolute differences in $|Z|$ before and after hybridization:

$$Signal = \frac{\sum_f Abs(|Z|_f^{after} - |Z|_f^{before}}{\max Z''_{before} \cdot N} \qquad (4)$$

To account for all available data, the sum is taken over all frequencies of the measurement. To account for differences between individual electrodes, the signal is normalized by the number of data points N and the maximum of the phase shift in the semicircle portion of the impedance spectrum before hybridization. The procedure is illustrated in Fig. 4 for two experiments using a noncomplementary target sequence (Fig. 4A) and a complementary target sequence (Fig. 4B). The star denotes the normalization factor max Z''_{before}, which is related to the electron transfer resistance of the electronic equivalent circuit shown in Fig. 1B, max $Z''_{before} = R_{ct}$ [22]. The formation of the cumulative sum in dependence of frequency is illustrated in Fig. 4C for the detection event (upper curve) and for a nondetection event (lower curve), giving a signal of approximately 80 kΩ for the detection event and 4 kΩ for a nondetection event. The normalized unitless signals are 0.9296 and 0.0447, respectively. For the following experiments, the normalized signal is reported solely.

The influence of spacer length

The oligonucleotide probe HA23 was attached at the end of each spacer, which was attached via a 6-carbon chain to a sulfhydryl group as shown in Fig. 2. The 6-carbon chain is of the same length as mercaptohexanol, which was used for backfilling to block nonspecific interactions with the gold electrode. For each spacer, the biosensor signal was obtained by incubation of the probe with either fully complementary target (cHA23 [Table 1]) or noncomplementary target (cMA20). The average biosensor signal from at least three experiments for all spacer molecules varied from 0.20 ± 0.11 to 0.71 ± 0.30 for treatment with complementary target and from 0.021 ± 0.032 to 0.12 ± 0.08 for treatment with noncomplementary target. The average results shown in Fig. 5 reveal a clear change of the signal for complementary target, whose magnitude varies with spacer length. In contrast, the signal for noncomplementary target is similar for all spacer

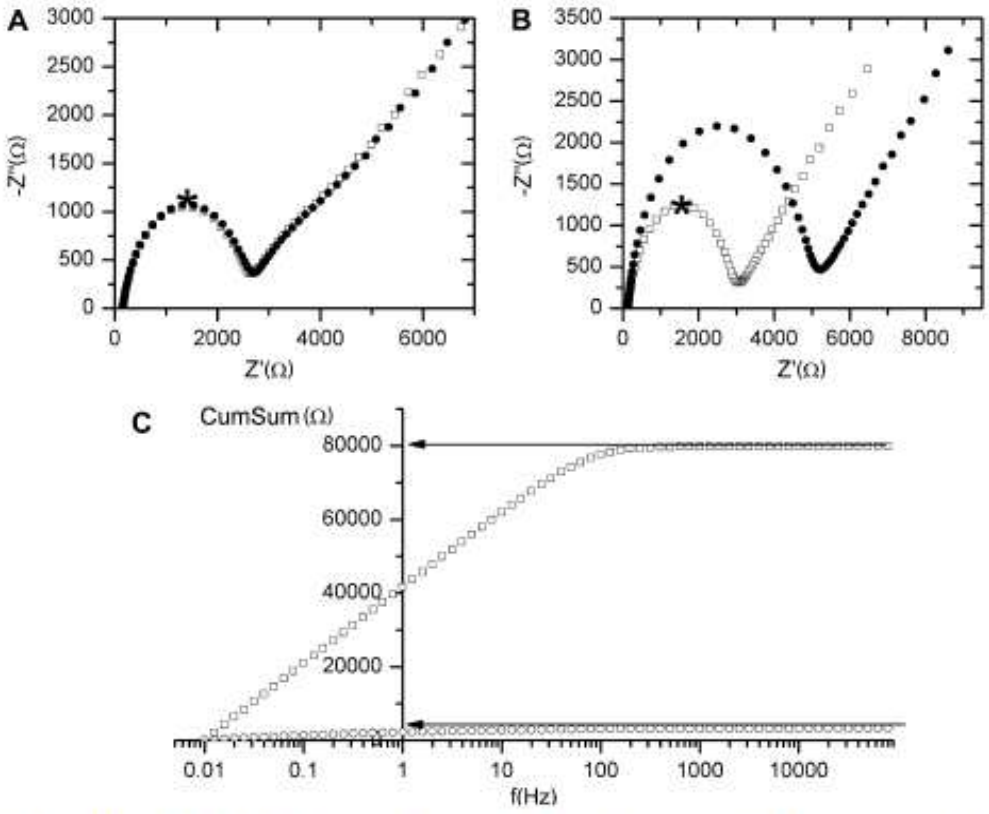

Fig. 4. Illustration of model-free data analysis. (A) EIS before (○) and after (●) treatment of the sensor with a noncomplementary target. (B) EIS before (○) and after (●) treatment with a complementary target. (C) Frequency dependence of the cumulative sum (CumSum) of the differences in the modulus |Z| of the EIS curves for treatment with a complementary target (upper curve) and treatment with a noncomplementary target (lower curve). The arrows point at the magnitude of the signal before normalization. For normalization, the signal is divided by the number of data points and by the maximum of $-Z''$ in the semicircle part of the EIS highlighted with a star in panels A and B.

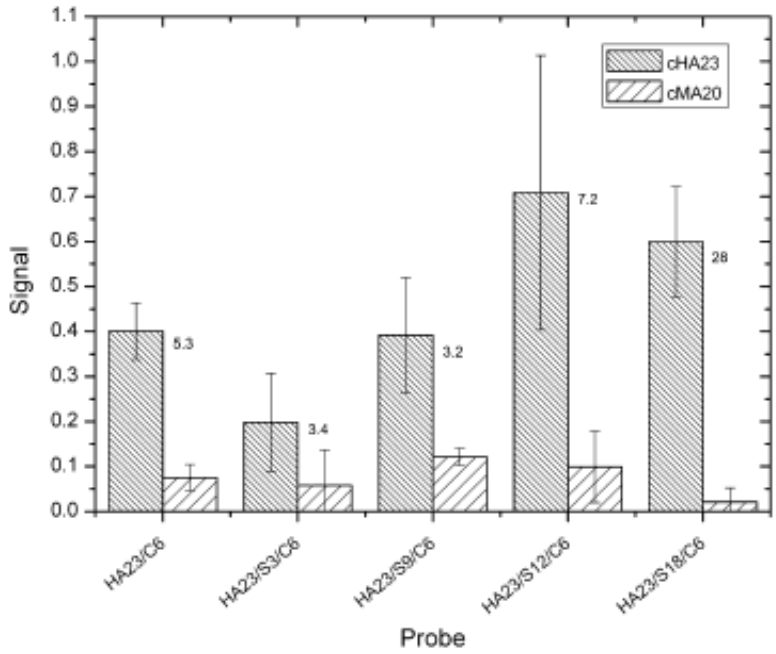

Fig. 5. Influence of spacer molecules. The dependence of the signal for the HA23 oligonucleotide attached to the gold surface with various spacer molecules treated with a complementary target and a noncomplementary target. Signal averages of at least three experiments are shown. The ratio of specific/nonspecific signal is given for each spacer molecule.

lengths investigated. Some spacer molecules are clearly unsuitable for biosensing of oligonucleotide hybridization (e.g., HA23/S3/C6). In contrast, HA23/S12/C6 gives the highest signal, followed by HA23/S18/C6, which also gives the highest ratio of specific/nonspecific signal (Fig. 5). However, only in a limited number of cases were we able to obtain stable SAMs with the HA23/S18/C6 probe, possibly indicating problems in synthesis of the longer spacer element; thus, we chose HA23/S12/C6 for further experiments.

Dependence on target concentration

Fig. 6A shows the dependence of the biosensing signal for the HA23/S12/C6 probe in dependence of the complementary target concentration cHA23. The dashed line indicates the level of signal after treatment with noncomplementary sequence at a concentration of 1000 nM. The detection limit is between 3 and 10 nM cHA23 when the signal exceeds the signal for noncomplementary sequence. The signal increases steeply between 3 and 30 nM, whereas there is no clear increase in signal between 30 and 1000 nM, but the fluctuations are within the error margin. The curve has been fitted with a classical binding curve (see Materials and Methods), yielding a maximum signal of $S_{max} = 0.70 \pm 0.01$, whereas the phenomenological dissociation constant is $K_D = 13.4 \pm 4$ nM and the exponent is $r = 1.31 \pm 0.08$, which is close to a value expected for a 1:1 complex. The dissociation constant compares well with K_D = 6.8 nM obtained from the on/off rate constant for hybridization of a 19-nt oligonucleotide target to a 19-nt surface-attached probe [37]. The detection limit is between 3 and 10 nM target molecules in 20 µl of solution, the volume used to cover the gold electrode surface, corresponding to 60 to 200 fmol of target molecules.

Detection of long target sequences

To test the ability of the biosensor to detect larger gene fragments as they may occur in samples taken from infected birds, we investigated the detection of a 120-mer target sequence containing 23 nucleotides reverse complementary to the probe HA23/S12/C6 (Fig. 6B). The average signal obtained with 1000 nM cHA120 target is 0.56, a value lower than that obtained with cHA23. The detection limit is in the region of 10 nM target concentration, corresponding to 200 fmol of target molecules.

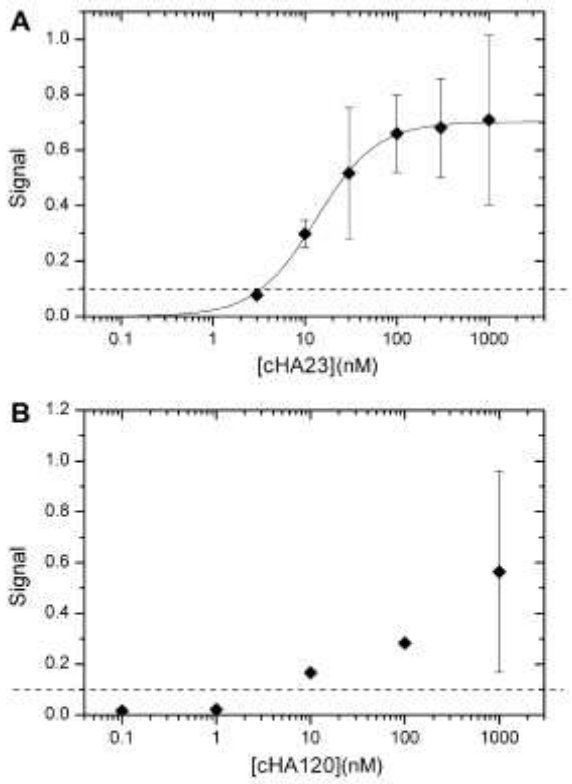

Fig. 6. Concentration dependence. (A) Dependence of the detection signal on the target concentration of cHA23 for the probe HA23/S12/C6. Averages of at least three experiments are shown. The line of best fit was obtained from the binding curve described in Eq. (2). (B) Demonstration of the ability to detect the 120mer target cHA120 with the probe HA23/S12/C6 at target concentration of 1000 nM. The level of signal for lower target concentrations also is shown. Note that error bars for concentrations below 1000 nM are not displayed for this proof-of-concept experiment. The dashed lines indicate the level of signal obtained with 1000 nM of the noncomplementary target cMA20.

Discussion

The appearance of a prominent semicircle in the EIS on treatment of the gold electrode with mercaptohexanol/HS-oligonucleotide (1:10) is indicative of the formation of a SAM. It has been shown that native DNA has a high affinity for gold and may adsorb nonspecifically to the gold surface [38]. To reduce nonspecific adsorption, we treated the gold electrode with a buffer containing a high concentration of mercaptohexanol (backfilling) and also used a 10:1 molar ratio of mercaptohexanol to probe DNA. Other molar ratios did not lead to a successful SAM formation (see supplementary material). The reduction of the charge transfer resistance on backfilling (Fig. 1A) indicates that backfilling is effective in reducing nonspecific adsorption, as is using mercaptohexanol in the initial step of electrode preparation. For samples taken in the field, a nucleic acid extraction step, which reduces the amount of protein and cellular material that may bind nonspecifically to gold electrodes, may be included. Alternatively, an ethyleneglycolcapped thiol, which has been reported to have very low protein and cellular adsorptivity, could be used [39]. The large variation in charge transfer resistance between various electrodes is caused by the manual steps of polishing (see Materials and Methods) and variations in the gold surface between electrodes that lead to a variation in surface properties at the molecular level, thereby influencing SAM formation. However, for the detection of hybridization, only the change of the curve or the magnitude of the derived detection signal is relevant. The devised biosensing system unequivocally demonstrates the detection of DNA sequences complementary to avian influenza gene probes. In particular, we propose using a 23-nt probe characteristic of high-virulence pathogenic strains (HA23) and a 20-nt probe characteristic of all influenza viruses (MA20); when taken together, these clearly would identify a highly pathogenic influenza virus despite the presence of genes from other organisms that might be present in an environmental sample. For a mobile device with limited computational power used by an unskilled operator, the automated data analysis resulting in a single numerical output (the signal) will be useful. In addition, the automated data analysis does not require a model of an electrical equivalent circuit, which might not be valid for all types of electrodes even if they are manufactured to a high standard. The model-free data analysis described here yields a signal whenever there is a change in the EIS.

To optimize the detection system, the influence of various spacer molecules shown in Fig. 2 on the detection signal was investigated. The results in Fig. 5 show that some spacer molecules are less suitable or completely unsuitable (e.g., HA23/S3/C6) given that the error margin of the detection signal with complementary target overlaps with the error margin of the signal in the presence of noncomplementary target. HA23/S12/C6 gives the highest detection signal, followed by HA23/S18/C6. In general, longer spacer molecules give a higher hybridization signal. The reason for

this may be the increased mobility of the probe, making it more readily available for hybridization. Once hybridized, the resulting highly charged duplex DNA is able to cover a wider area of the surface, leading to increased electrostatic repulsion of the negatively charged redox marker. Interestingly, the error margins between detection of complementary sequence and detection of noncomplementary sequence are further apart for HA23/ S18/C6 than for HA23/S12/C6, and this would render this spacer as equally suitable for a detection device. It would be interesting to investigate whether longer spacers lead to further improvements, although the chemistry currently is not available to us.

The concentration dependence of the detection signal shows a detection limit below 200 fmol of target molecule, with a macroscopic gold electrode using a buffer volume of 20 µl to cover the gold surface. For the current experimental setup, the volume could be reduced to 10 µl, thereby reducing the detection limit of the number of target molecules even further. Because the detection limit depends on the area of the electrodes, we would expect a lower detection limit for electrodes used in a microarray device. In addition, much lower sample volumes are required to cover a microelectrode. Current DNA microarrays for optical detection use volumes in the picoliter range; for example, for 100 pl, the theoretical detection limit would be reduced to 1 amol (i.e., ~ 6×10^5 molecules), which compares well with typical viral loads of 10^5 to 10^6 copy numbers found in oropharyngeal samples [40]. In addition, the current hybridization time of 2 h would be reduced. However, the EIS for smaller electrodes may be limited by noise effects and contributions from the edges of electrodes that become more prominent if the electrode surface is reduced; thus, amplification by RT–PCR might be necessary.

The detection limit of the currently most sensitive rRT– PCR method has been reported to be between 5 and 50 RNA copies per reaction [12], which is substantially lower than the detection limit reported in the current work. However, compared with a multiplex rRT–PCR system, a microarray EIS system would have the advantage of a smaller size, provide more information, provide faster readout times, and potentially possess a disposable sensor element that reduces the risk of spreading the virus.

The concentration dependence of the signal follows a classical binding curve, whereas the exponent in the region of $r \approx 1$ indicates a 1:1 complex formation between probe and target, as would be expected for the formation of a DNA duplex from single-stranded oligonucleotides. However, the binding curve is a phenomenological description of the concentration dependence of the signal. The actual binding may be a stepwise process in which shorter stretches of base pairs are formed in succession, explaining the noninteger value of $r = 1.3$ obtained.

The detection signal for a short (23-nt) oligonucleotide is higher than that for a longer (120-nt) oligonucleotide containing the 23-nt sequence within it. This might be caused by the space constraints on the sensor surface. Once the DNA duplex is formed, nonhybridized stretches of DNA approximately 50 nt long remain on each side, and this may prevent hybridization at neighboring probe molecules. In addition, the hybridization efficiency of such a long target may be lower than that of a short, completely matched target taking into account the 50-nt overhang on the 50 end close to the gold surface. This also would explain why the detection limit of at least 10 nM is higher for the 120-mer target than for the 23-mer target. These observations have strong implications for the design of DNA microarrays. Although longer oligonucleotide probes may confer greater specificity, shorter oligonucleotides may give rise to greater sensitivity. Because the microarray format allows specificity to be determined from combinations of oligonucleotide probes as discussed here, shorter oligonucleotides may prove to be the probes of choice. There are also implications for sample preparation; techniques designed to maintain sample (e.g., RNA, DNA) integrity may be detrimental to signal generation if short ligands are preferred.

Conclusions

We have used an optimized procedure for SAM formation on gold electrodes that employs a 1:10 DNA/mercaptohexanol ratio, followed by backfilling with mercaptohexanol alone (see supplementary material). A systematic investigation of the spacer molecule between the oligonucleotide and the gold surface identified HA23/S12/C6 or HA23/S18/C6 (see Fig. 2) as the optimal length.

With these probes, we showed the detection of a 23-nt DNA sequence as a model for an avian influenza gene sequence to a detection limit below 200 fmol. These results form the basis for the development of a portable gold microelectrode array device using the impedimetric detection principle that is able to analyze environmental samples for the presence of highly pathogenic avian influenza virus strains that may present a risk to humans.

Acknowledgments

The authors thank Michael Helmus of Advance Nanotech for pointing out the importance of label-free detection in the field of avian influenza and for engaging in helpful discussions. Special thanks go to Simon Keighley for optimizing the procedure for the preparation of electrodes, assisting with measurement, and providing helpful suggestions for the manuscript. This work was supported by Advance Nanotech, in partnership with the Centre for Advanced Photonics and Electronics (CAPE) of the Department of Engineering, University of Cambridge, under the BiMAT project. P.E. acknowledges support from the BBSRC under contract BB/D523094/1. Work in the P.K-F. lab was supported by a grant-in-aid from the Medical Research Council to the Cancer Cell Unit. A.K. and P.K-F. acknowledge the generous support of the Hutchison/ MRC Research Centre and Cancer Cell Unit, where some of the work was performed.

References

[1] J.C. Obenauer, J. Denson, P.K. Mehta, X. Su, S. Mukatira, D.B. Finkelstein, X. Xu, J. Wang, J. Ma, Y. Fan, K.M. Rakestraw, R.G. Webster, E. Hoffmann, S. Krauss, J. Zheng, Z. Zhang, C.W. Naeve, Large-scale sequence analysis of avian influenza isolates, Science 311 (2006) 1576–1580.

[2] D. Kobasa, Y. Kawaoka, Emerging influenza viruses: Past and present, Curr. Mol. Med. 5 (2005) 791–803.

[3] J. Li, S. Chen, D.H. Evans, Typing and subtyping influenza virus using DNA microarrays and multiplex reverse transcriptase PCR, J. Clin. Microbiol. 39 (2001) 696–704.

[4] N.P. Johnson, J. Mueller, Updating the accounts: Global mortality of the 1918–1920 ‘‘Spanish’’ influenza pandemic, Bull. Hist. Med. 76 (2002) 105–115.

[5] N.J. Cox, K. Subbarao, Global epidemiology of influenza: Past and present, Annu. Rev. Med. 51 (2000) 407–421.

[6] T. Horimoto, Y. Kawaoka, Influenza: Lessons from past pandemics, warnings from current incidents, Nat. Rev. Microbiol. 3 (2005) 591–600.

[7] E.C. Claas, A.D. Osterhaus, R. van Beek, J.C. De Jong, G.F. Rimmelzwaan, D.A. Senne, S. Krauss, K.F. Shortridge, R.G. Webster, Human influenza A H5N1 virus related to a highly pathogenic avian influenza virus, Lancet 351 (1998) 472–477.

[8] K. Subbarao, A. Klimov, J. Katz, H. Regnery, W. Lim, H. Hall, M. Perdue, D. Swayne, C. Bender, J. Huang, M. Hemphill, T. Rowe, M. Shaw, X. Xu, K. Fukuda, N. Cox, Characterization of an avian influenza A (H5N1) virus isolated from a child with a fatal respiratory illness, Science 279 (1998) 393–396.

[9] World Health Organization, Avian influenza A (H5N1), Weekly Epidemiol. Rec. 79 (7) (2004) 65–70.

[10] G.A. Storch, Essentials of Diagnostic Virology, Churchill Livingstone, New York, 2000.

[11] S. Payungporn, S. Chutinimitkul, A. Chaisingh, S. Damrongwantanapokin, C. Buranathai, A. Amonsin, A. Theamboonlers, Y. Poovorawan, Single step multiplex real-time RT–PCR for H5N1 influenza A virus detection, J. Virol. Methods 131 (2006) 143–147.

[12] L. Di Trani, B. Bedini, I. Donatelli, L. Campitelli, B. Chiappini,M.A. De Marco, M. Delogu, C. Buonavoglia, G. Vaccari, A sensitive onestep real-time PCR for detection of avian influenza viruses using a MGB probe and an internal positive control, BMC Infect. Dis. 6 (2006) 87.

[13] E. Spackman, D.A. Senne, T.J. Myers, L.L. Bulaga, L.P. Garber, M.L. Perdue, K. Lohman, L.T. Daum, D.L. Suarez, Development of a real-time reverse transcriptase PCR assay for type A

influenza virus and the avian H5 and H7 hemagglutinin subtypes, J. Clin. Microbiol. 40 (2002) 3256–3260.

[14] S. Payungporn, P. Phakdeewirot, S. Chutinimitkul, A. Theamboonlers, J. Keawcharoen, K. Oraveerakul, A. Amonsin, Y. Poovorawan, Single-step multiplex reverse transcription–polymerase chain reaction (RT–PCR) for influenza A virus subtype H5N1 detection, Viral Immunol. 17 (2004) 588–593.

[15] B. Hoffmann, T. Harder, E. Starick, K. Depner, O. Werner, M. Beer, Rapid and highly sensitive pathotyping of avian influenza A H5N1 virus by using real-time reverse transcription–PCR, J. Clin. Microbiol. 45 (2007) 600–603.

[16] G.R. Risatti, J.D. Callahan, W.M. Nelson, M.V. Borca, Rapid detection of classical swine fever virus by a portable real-time reverse transcriptase PCR assay, J. Clin. Microbiol. 41 (2003) 500–505.

[17] E.D. Dawson, C.L. Moore, J.A. Smagala, D.M. Dankbar, M. Mehlmann, M.B. Townsend, C.B. Smith, N.J. Cox, R.D. Kuchta, K.L. Rowlen, MChip: A tool for influenza surveillance, Anal. Chem. 78 (2006) 7610–7615.

[18] M.B. Townsend, E.D. Dawson, M. Mehlmann, J.A. Smagala, D.M. Dankbar, C.L. Moore, C.B. Smith, N.J. Cox, R.D. Kuchta, K.L. Rowlen, Experimental evaluation of the FluChip diagnostic microarray for influenza virus surveillance, J. Clin. Microbiol. 44 (2006) 2863–2871.

[19] A.L. Ghindilis, M.W. Smith, K.R. Schwarzkopf, K.M. Roth, K. Peyvan, S.B. Munro, M.J. Lodes, A.G. Stover, K. Bernards, K. Dill, A. McShea, CombiMatrix oligonucleotide arrays: Genotyping and gene expression assays employing electrochemical detection, Biosens. Bioelectron. 22 (2007) 1853–1860.

[20] R.H. Liu, M.J. Lodes, T. Nguyen, T. Siuda, M. Slota, H.S. Fuji, A. McShea, Validation of a fully integrated microfluidic array device for influenza A subtype identification and sequencing, Anal. Chem. 78 (2006) 4184–4193.

[21] M.J. Lodes, D. Suciu, M. Elliott, A.G. Stover, M. Ross, M. Caraballo, K. Dix, J. Crye, R.J. Webby, W.J. Lyon, D.L. Danley, A. McShea, Use of semiconductor-based oligonucleotide microarrays for influenza A virus subtype identification and sequencing, J. Clin. Microbiol. 44 (2006) 1209–1218.

[22] E. Katz, I. Willner, Probing biomolecular interactions at conductive and semiconductive surfaces by impedance spectroscopy: Routes to impedimetric immunosensors, DNA-sensors, and enzyme biosensors, Electroanalysis 15 (2003) 913–947.

[23] H.G.L. Coster, T.C. Chilcott, A.C.F. Coster, Impedance spectroscopy of interfaces, membranes, and ultrastructures, Bioelectrochem. Bioenerg. 40 (1996) 79–98.

[24] H. Aoki, P. Bu¨hlmann, Y. Umezawa, Electrochemical detection of a one-base mismatch in an oligonucleotide using ion-channel sensors with self-assembled PNA monolayers, Electroanalysis 12 (2000) 1272–1276.

[25] S. Nagase, M. Kataoka, R. Nanganawa, R. Komatsu, K. Odashima, Y. Umezawa, Voltammetric anion responsive sensors based on modulation of ion permeability through Langmuir–Blodgett films containing synthetic anion receptors, Anal. Chem. 62 (1990) 1252–1259.

[26] V. Dharuman, T. Grunwald, E. Nebling, J. Albers, L. Blohm, R. Hintsche, Label-free impedance detection of oligonucleotide hybridisation on interdigitated ultramicroelectrodes using electrochemical redox probes, Biosens. Bioelectron. 21 (2005) 645–654.

[27] V. Dharuman, E. Nebling, T. Grunwald, J. Albers, L. Blohm, B. Elsholz, R. Worl, R. Hintsche, DNA hybridization detection on electrical microarrays using coulostatic pulse technique, Biosens. Bioelectron. 22 (2006) 744–751.

[28] National Center for Biotechnology Information, Influenza Virus Resource, Bethesda, MD, 2004.

[29] T.A. Hall, BioEdit [software] (2005).

[30] T.A. Hall, BioEdit: A user friendly biological sequence alignment editor and analysis program for Windows 95/98/NT, Nucleic Acids. Symp. Ser. 41 (1999) 95–98.

[31] R.C. Edgar, MUSCLE: A multiple sequence alignment method with reduced time and space complexity, BMC Bioinformatics 5 (2004) 113.

[32] R.C. Edgar, MUSCLE: Multiple sequence alignment with high accuracy and high throughput, Nucleic Acids Res. 32 (2004) 1792–1797.

[33] A. Stieneke-Grober, M. Vey, H. Angliker, E. Shaw, G. Thomas, C. Roberts, H.D. Klenk, W. Garten, Influenza virus hemagglutinin with multibasic cleavage site is activated by furin, a subtilisin-like endoprotease, EMBO J. 11 (1992) 2407–2414.

[34] J.E.B. Randles, Kinetics of rapid electrode reactions, Discuss. Faraday Soc. 1 (1947) 11–19.

[35] B.V. Ershler, Discuss. Faraday Soc. 1 (1947) 269.

[36] A.J. Bard, L.R. Faulkner, Electrochemical Methods: Fundamentals and Applications, John Wiley, New York, 1980.

[37] D. Li, X. Zou, Q. Shen, S. Dong, Kinetic study of DNA/DNA hybridisation with electrochemical impedance spectroscopy, Electrochem. Commun. 9 (2007) 191–196.

[38] A.B. Steel, R.L. Levicky, T.M. Herne, M.J. Tarlov, Immobilization of nucleic acids at solid

surfaces: Effect of oligonucleotide length on layer assembly, Biophys. J. 79 (2000) 975–981.

[39] E. Ostuni, R.G. Chapman, M.N. Liang, G. Meluleni, G. Pier, D.E. Ingeber, G.M. Whitesides, Self-assembled monolayers that resist the adsorption of proteins and the adhesion of bacterial and mammalian cells, Langmuir 17 (2001) 6336–6343.

[40] H. Toro, D.C. Tang, D.L. Suarez, M.J. Sylte, J. Pfeiffer, K.R. Van Kampen, Protective avian influenza in ovo vaccination with nonreplicating human adenovirus vector, Vaccine 25 (2007) 2886–2891.

[41] C.S. Hsu, F. Mansfield, Concerning the conversion of the constant phase element parameter Y0 into a capacitance [technical note], Corrosion 57 (2001) 747–748.

Appendix A. Supplementary data

Optimization of the ssDNA immobilization protocol

Different ssDNA immobilization protocols have been attempted in a separate study and will be reported elsewhere [1]. Co-immobilization of thiolated ssDNA with mercaptohexanol (MCH) renders considerably better self-assembled monolayers (SAMs) compared to the case where ssDNA is immobilized alone followed by backfilling with MCH.

The relative ratio between ssDNA and MCH used upon immobilization also plays an important role in the selectivity of the DNA SAM. When ssDNA is co-immobilized with MCH in a 1:1 molar ratio, the charge transfer resistance R_{ct} decreases upon hybridization (see Figure A). An increase of the value of R_{ct} is instead expected, since the negative charge of the DNA layer increases upon hybridization, resulting in a stronger electrostatic repulsion for the negatively charged $[Fe(CN)_6]^{3-/4-}$ redox markers. Figure B shows the results before and after hybridization for a ssDNA layer co-immobilized with MCH in a molar ratio of 1:10. The value of R_{ct} for ssDNA is considerably lower than in Figure A. Upon hybridization R_{ct} increases, as expected [2].

The reduction in R_{ct} for increasing MCH/ssDNA ratio can be explained with the fact that in the case of figure A a significant amount of ssDNA probes lie flat on the surface, whereas in the case of figure B the oligomers have an almost vertical orientation. The electrostatic repulsion for the redox markers is stronger in the former case as the DNA charge is distributed over a larger portion of surface. In this case, the reduction of R_{ct} upon hybridization can be justified by the fact that the formation of the DNA duplex forces it to desorb from the Au surface and attain a perpendicular position with respect to the surface. This configuration will result in a weaker electrostatic barrier to the redox markers. It is therefore very important to optimise the MCH/ssDNA molar ratio, to achieve the correct SAM structure and assay specificity. After co-immobilization of ssDNA and MCH, the quality of the SAM can be further improved by backfilling with concentrated MCH.

[1] Keighley SD, Li P, Estrela P, Migliorato P: manuscript in preparation.

[2] See e.g. Patolsky F, Lichtenstein A, Willner I: *Angew. Chem. Int. Ed.* 2000, 39(5):940-943 and references within.

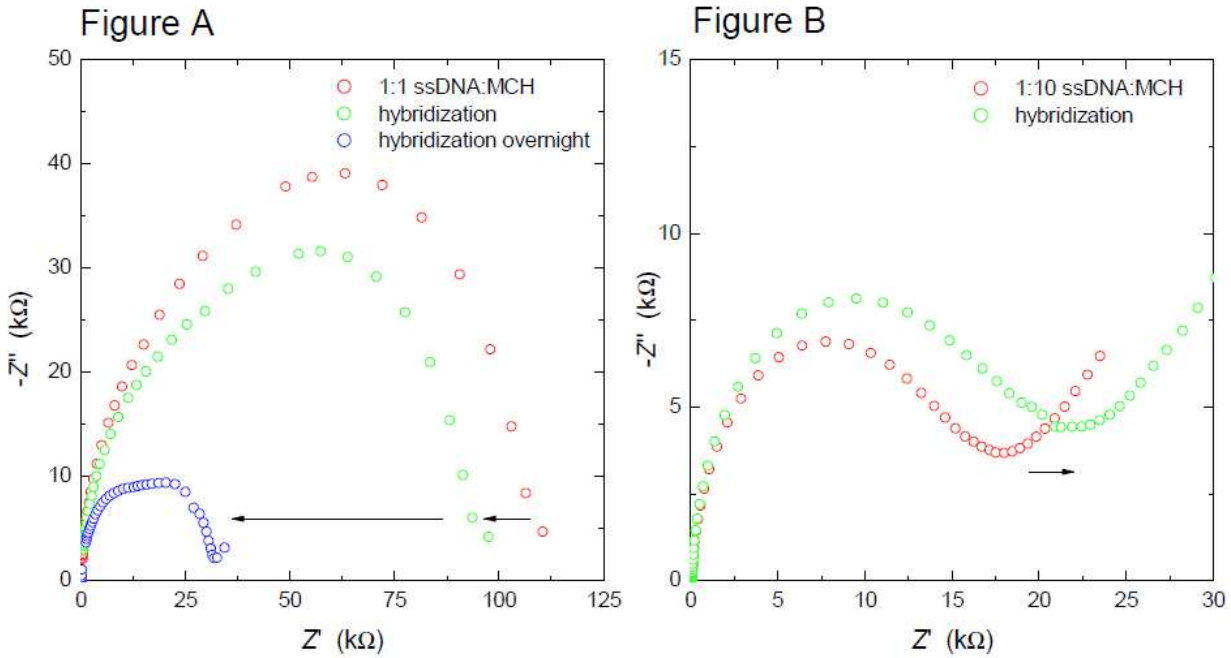

Figure A - Nyquist plot of EIS spectra for ssDNA co-immobilized with MCH in a 1:1 molar ratio.
The figure shows the spectra obtained in 100 mM phosphate buffer (PB) with 5 mM $K_3Fe(CN_6)$ and 5 mM $K_4Fe(CN_6)$ after: a) overnight immobilization of 1 μM ssDNA (20-mer) and 1 μM MCH in 0.8 M PB pH 7.0 with 1 M NaCl and 5 mM $MgCl_2$; b) hybridization with 5 μM of the complementary strand in 1 M PB with 50 mM NaCl for 40 min; c) overnight hybridization with 5 μM of the complementary strand.

Figure B - Nyquist plot of EIS spectra for ssDNA co-immobilized with MCH in a 1:10 molar ratio.
The figure shows the spectra obtained in the same buffer conditions as in Figure A after: a) overnight immobilization of 1 μM ssDNA and 10 μM MCH; b) hybridization with 1 μM of the complementary strand for 30 min.